Simultaneous Enhancement of the Strength and Elongation of Polycaprolactone: The Role of Chitosan-*graft*-Polycaprolactone

Ziyan Zhou,[1,2] Haitao Huang,[2] Peihu Xu,[2] Lihong Fan,[2] Jiahui Yu,[1] Jin Huang[1,2,3]

[1]*College of New Drug Innovation Research and Development, East China Normal University, Shanghai 200062, China*
[2]*College of Chemical Engineering and Affiliated Hospital, Wuhan University of Technology, Wuhan 430070, China*
[3]*Key Laboratory of Cellulose and Lignocellulosics Chemistry, Guangzhou Institute of Chemistry, Chinese Academy of Sciences, Guangzhou 510650, China*

Received 2 May 2008; accepted 7 October 2008
DOI 10.1002/app.29432
Published online 13 January 2009 in Wiley InterScience (www.interscience.wiley.com).

ABSTRACT: Polycaprolactone (PCL) is a basic substance for biomedical materials and especially for scaffolds in tissue engineering. To improve the performance of PCL-based materials, we filled a PCL matrix with a biocompatible polysaccharide-grafted PCL, chitosan-*g*-polycaprolactone (CS-*g*-PCL). The results showed that the strength, elongation, and Young's modulus of the resultant composites were simultaneously enhanced in contrast with those of neat PCL. The structures of the PCL/CS-*g*-PCL blends were investigated with Fourier transform infrared, X-ray diffraction, differential scanning calorimetry, dynamic mechanical analysis, and scanning electron microscopy, and the effects of the chitosan (CS) content in CS-*g*-PCL and the CS-*g*-PCL content in the blends on the mechanical properties and structures of the blends were examined. The rigidity of CS chains and the increasing crystallinity induced by the nucleation of CS-*g*-PCL contributed to the enhancement of the strength, whereas the cocontinuous interfacial structure and improved miscibility between CS and PCL matrix mediated with grafted PCL chains greatly enhanced the elongation of the composite materials. This work presents a strategy for enhancing the mechanical performance of PCL as a biomaterial. © 2009 Wiley Periodicals, Inc. J Appl Polym Sci 112: 692–699, 2009

Key words: blends; graft copolymers; mechanical properties

INTRODUCTION

Natural chitosan (CS)[1–6] and chemosynthetic polycaprolactone (PCL)[7–12] are well sought after as substances in biomedical applications, such as biomedical devices, wound healing, controlled drug delivery, and tissue engineering, because of their biocompatibility and biodegradability as well as the antimicrobial properties of CS. CS has sparked interest in the field of tissue engineering as a scaffold material because of some additional advantages, such as its processability into a desired porous configuration[13] and its positive charge and polar groups, which facilitate its structural modification and interaction with other molecules. However, despite these advantages, current use in tissue engineering is limited mainly by the low strength and incomplete understanding of cellular interactions with CS. Although PCL exhibits excellent tensile properties,[14,15] the applications of PCL in tissue engineering have been restricted by the disadvantages of its poor bioregulatory activity, which is primarily due to its highly hydrophobic nature, slow biodegradation rate, and susceptibility to microbial action. It is worth noting that the versatility of PCL in blending with other polymers allows the improvement of its properties to overcome such drawbacks because of its flexibility under ambient conditions,[16–18] which is determined by its moderate melting point and low glass-transition temperature.

As a result, hydrophilic CS and hydrophobic PCL have been compounded together to exploit novel biomaterials.[19–24] In addition to basic studies on the

Correspondence to: J. Yu (yujh109@yahoo.com.cn) and J. Huang (huangjin@iccas.ac.cn).

Contract grant sponsor: National Nature Science Foundation of China; contract grant numbers: 20504010 and 50843031.
Contract grant sponsor: Youth Chenguang Program of Science and Technology in Wuhan; contract grant number: 200850731383.
Contract grant sponsor: Chinese Ministry of Science and Technology (a 973 project); contract grant number: 2009CB930000.
Contract grant sponsor: State Key Laboratory of Pulp and Paper Engineering, South China University of Technology; contract grant numbers: 200514 and 200716.
Contract grant sponsor: Key Laboratory of Cellulose and Lignocellulosics Chemistry, Guangzhou Institute of Chemistry, Chinese Academy of Sciences; contract grant numbers: LCLC-2005-172 and LCLC-2008-02.

structure and physicochemical properties of CS/PCL blends, the blends have been verified to be nontoxic[22] and hence have been developed as porous scaffolds for tissue engineering.[23,24] Although the blends inherit the functional properties of PCL and CS, the mechanical performances of the blends decrease in contrast with neat PCL, and even the elongation is lower than that of neat CS.[24] Thus, we must consider how to improve the miscibility between CS and PCL. Currently, the graft copolymerization of ε-caprolactone (CL) with CS has been extensively investigated.[25–31] PCL chains grafted onto CS can drive the dissolution of CS in organic solvents, such as CH_2Cl_2, a good solvent for PCL, in order to produce a homogeneous blend in the process of solvent mixing. At the same time, the grafted PCL chains might improve the miscibility between the CS and PCL matrix because the grafted chains and PCL matrix have the same origin. In this work, we synthesized chitosan-*g*-polycaprolactone (CS-*g*-PCL) by microwave-assisted ring-open polymerization and then compounded it into PCL to produce blend films by solvent casting. The structure and mechanical properties of the resultant blends were investigated with Fourier transform infrared (FTIR) spectroscopy, X-ray diffraction (XRD), differential scanning calorimetry (DSC), dynamic mechanical analysis (DMA), scanning electron microscopy (SEM), and tensile tests. Moreover, high mechanical performances of the blends were expected, and so the key role of grafted PCL chains was examined.

EXPERIMENTAL

Materials

CS from shrimp shells was kindly provided by Yuhuan Ocean Biochemical Co. (Zhejiang, China), and its number-average molecular weight and deacetylation degree were 78.1×10^4 and 95.5%, respectively. PCL with a number-average molecular weight of 42,500 was purchased from Aldrich. CL monomer was purchased from Alfa Aesar and used as received. Tin(II) octoate [$Sn(Oct)_2$] and other analytical-grade reagents were purchased from the Shanghai Sinopharm Chemical Co., Ltd. (Shanghai, China), and used as received.

Synthesis of CS-*g*-PCL

A mixture of CS and CL with a given weight ratio was placed in a round-bottom reactor, and this was followed by the addition of $Sn(Oct)_2$ (0.5% with respect to the weight of CL). Thereafter, the reactant was homogenized with a Lab Dancer compact shaker (IKA, Germany) and then vacuum-exhausted for 30 min. Subsequently, the reactor containing the reactant was conditioned under 225 W of microwave radiation for 3 min. The crude product was first dissolved into CH_2Cl_2, and then CH_3OH was added drop by drop to obtain white precipitates. At last, the precipitates were vacuum-dried for 24 h after being washed with a CH_3OH/H_2O mixture three times. According to the feed weight ratio of CS to CL (listed in parentheses after the codes), the resulting CS-*g*-PCLs were coded as CS-*g*-PCL(I) (1 : 25), CS-*g*-PCL(II) (1 : 20), and CS-*g*-PCL(III) (1 : 10).

Preparation of the PCL/CS-*g*-PCL blends

CS-*g*-PCLs with various compositions were individually dissolved in CH_2Cl_2 and then mixed with a given weight ratio of CS-*g*-PCL to PCL. The mixed solutions were cast into a Teflon mold, and this was followed by solidification at the ambient temperature for about 48 h. At last, all the solidified films with a thickness of about 0.15 mm were vacuum-dried until constant weights were obtained in order to verify that no solvent was left in the films. All the films were transparent, showing a homogeneous structure. According to the origin of CS-*g*-PCL and the weight of CS-*g*-PCL in the blends, the blend films were coded as PC(I)-25, PC(I)-50, PC(I)-75, PC(II)-50, and PC(III)-50, where the numbers represent the weight percentages of CS-*g*-PCL in the blends. In addition, the neat PCL film was solidified from PCL dissolved in CH_2Cl_2.

Characterization

Elemental analysis of the CS-*g*-PCL and CS powders was conducted on a Vario EL III elemental analyzer (Elementar, Germany).

FTIR spectra of the CS and CS-*g*-PCL powders as well as all the films were also recoded on an FTIR 5700 spectrometer (Nicolet, United States). The powders were measured with a KBr pellet method in the range of 4000–400 cm^{-1}, and the films were scanned with Smart OMNT reflectance accessories in the range of 4000–700 cm^{-1}.

XRD measurements were performed on a D/max-2500 X-ray diffractometer (Rigaku Denki, Japan) with Cu $K\alpha_1$ radiation ($\lambda = 0.154$ nm) in the 2θ range of 3–60° with a fixed time mode with a step interval of 0.02°.

SEM observation was carried out on an S-3000N scanning electron microscope (Hitachi, Japan). The films were frozen in liquid nitrogen and then snapped immediately. The fractured surfaces of the films were sputtered with gold and then observed and photographed.

DSC analysis of the blend films and neat PCL film was carried out with a DSC-204 instrument (Netzsch, Germany) under a nitrogen atmosphere at

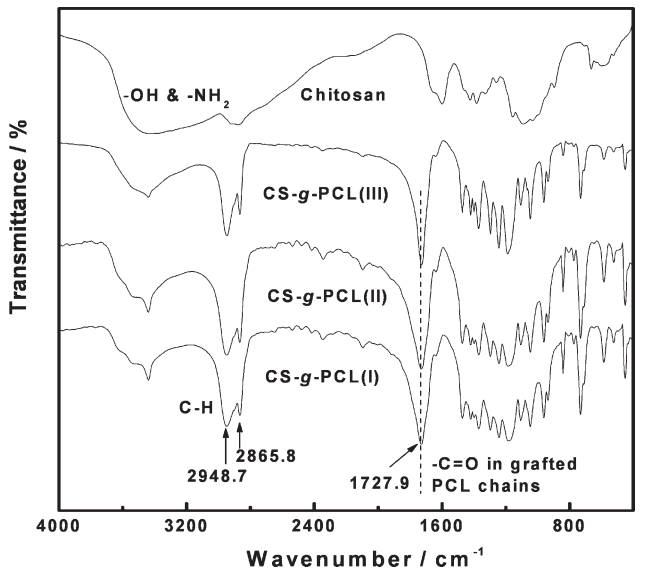

Figure 1 FTIR spectra of the CS-*g*-PCL powders and reference CS powder.

a heating or cooling rate of 20°C/min. The films were scanned in the range of −150–100°C after a pretreatment (heating from 20 to 100°C and then cooling to −150°C) used to eliminate the thermal history.

DMA was carried out on a DMA 242C dynamic mechanical analyzer (Netzsch, Germany) at a frequency of 1 Hz. The temperature ranged from −150 to 100°C with a heating rate of 3°C/min. Measurements were performed with a dual cantilever device, and the size of the testing samples was 40 × 10 mm^2.

The tensile strength, breaking elongation, and Young's modulus of the blend films and neat PCL film were measured on a universal testing machine (CMT6503, Shenzhen SANS Test Machine Co., Ltd., Shenzhen, China) with a tensile rate of 5 mm/min according to ISO 527-3 : 1995(E). The tested samples were cut into quadrate strips with a width of 10 mm, and the distance between testing marks was 40 mm. The tested strips were kept at 35% humidity for 7 days before the measurement. An average value of five replicates of each sample was taken.

RESULTS AND DISCUSSION

Structure and composition of CS-*g*-PCL

FTIR spectra of the CS-*g*-PCL and CS powders are depicted in Figure 1. In comparison with the spectrum of CS, there are two specific changes for the CS-*g*-PCLs: there are two distinct peaks at 2865.8 and 2948.7 cm^{-1} due to the methylene groups in grafted PCL chains, and a new strong absorption at 1727.9 cm^{-1} can be assigned to the ester carbonyl in grafted PCL chains.[26,27] Meanwhile, the absorption of —OH and —NH_2 vibrations above about 3000 cm^{-1} obviously decreased. This indicates that PCL and CS were successfully linked together to produce new graft copolymers by the initiation of —OH or —NH_2 groups. Furthermore, the content of the element carbon, measured from elemental analysis, was used to obtain the content of PCL in CS-*g*-PCL. The contents of carbon in CS-*g*-PCLs and CS were determined to be 61.39 [CS-*g*-PCL(I)], 60.64 [CS-*g*-PCL(II)], 59.76 [CS-*g*-PCL(III)], and 40.99% (CS), whereas the theoretical content of carbon in PCL was 63.16%. Consequently, the content of grafted PCL chains in CS-*g*-PCL was calculated with the following equation:

$$(1 - x)C_{PCL} + xC_{CS} = C_{CS-g-PCL}$$

where C_{PCL}, C_{CS}, and $C_{CS\text{-}g\text{-}PCL}$ are the contents of the element carbon in PCL, CS, and CS-*g*-PCL, respectively; and x is the weight percentage of CS in CS-*g*-PCL. The results showed that the CS content in CS-*g*-PCL was 7.98 [CS-*g*-PCL(I)], 11.37 [CS-*g*-PCL(II)], and 15.34 wt % [CS-*g*-PCL(III)], suggesting that the grafted PCL chains were the major component in CS-*g*-PCL.

Mechanical performance of the PCL/CS-*g*-PCL blends

The effects of the CS content in CS-*g*-PCL on the mechanical properties of the blend films with the equivalent weights of CS-*g*-PCL and PCL are depicted in Figure 2. Obviously, with a decrease in the CS content in CS-*g*-PCL, the tensile strength and breaking elongation simultaneously increased. At the same time, PCL(II)-50, containing CS-*g*-PCL(II) with a moderate CS content, showed the maximum value of Young's modulus. However, except for the lower breaking elongation of PC(III)-50 with the highest CS content, all the blend films showed

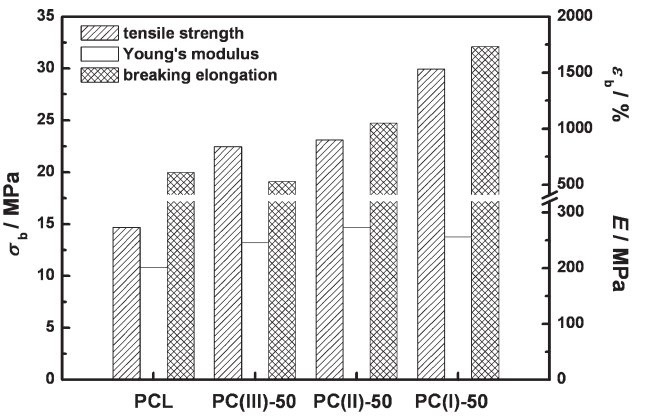

Figure 2 Mechanical properties of the PC blend films with the equivalent weight of CS-*g*-PCL and PCL based on various CS contents in CS-*g*-PCL (E = Young's modulus; σ_b = tensile strength; ε_b = breaking elongation).

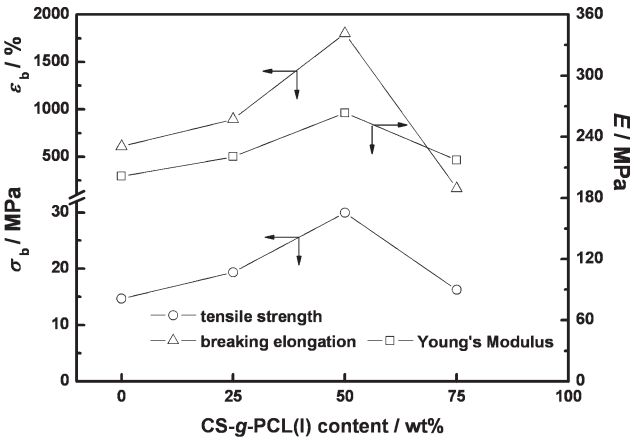

Figure 3 Effects of the CS-*g*-PCL(I) content on the mechanical properties of the blend PC(I) films (E = Young's modulus; σ_b = tensile strength; ε_b = breaking elongation).

enhanced tensile strength, Young's modulus, and breaking elongation in contrast with the neat PCL film, that is, simultaneous reinforcement and toughening. In particular, PC(I)-50, containing CS-*g*-PCL(I) with the lowest CS content, showed the maximum tensile strength of 29.9 MPa and the greatest elongation of 1733%; these were about 2-fold and 3-fold greater than those of the neat PCL film, respectively. In addition, the effects of the CS-*g*-PCL(I) content on the mechanical properties were further investigated. Figure 3 shows that the optimal CS-*g*-PCL(I) content was 50 wt %. As a result, the PC(I)-50 blend had the best mechanical performance of all the PCL/CS-*g*-PCL composites.

Structural analysis of the PCL/CS-*g*-PCL blends

XRD patterns of the PC blends as well as the neat PCL and CS powders are depicted in Figure 4. Compared with neat PCL, all the blends showed analogous diffraction patterns, which appeared as two typical crystalline peaks located at 2θ values of 22.20 and 23.96°. However, the diffraction peaks located at 2θ values of 11.04 and 20.06° for semicrystalline CS powder were submerged into the strong diffraction of the PCL component because of the low content of CS. As a result, all the blends showed characteristics typical of semicrystalline PCL on the whole.

In general, the vibration of groups in the FTIR spectrum of a semicrystalline polymer should be composed of at least two components arising from its crystalline and amorphous phases. As a result, the stretching vibration of —C=O, located at about 1727 cm^{-1} and assigned to the PCL component, was divided into crystalline and amorphous peaks by curve fitting. The fractions and locations of the crystalline and amorphous peaks are summarized in Table I, and the fraction of the crystalline peak is proportional to the crystalline degree. The crystalline

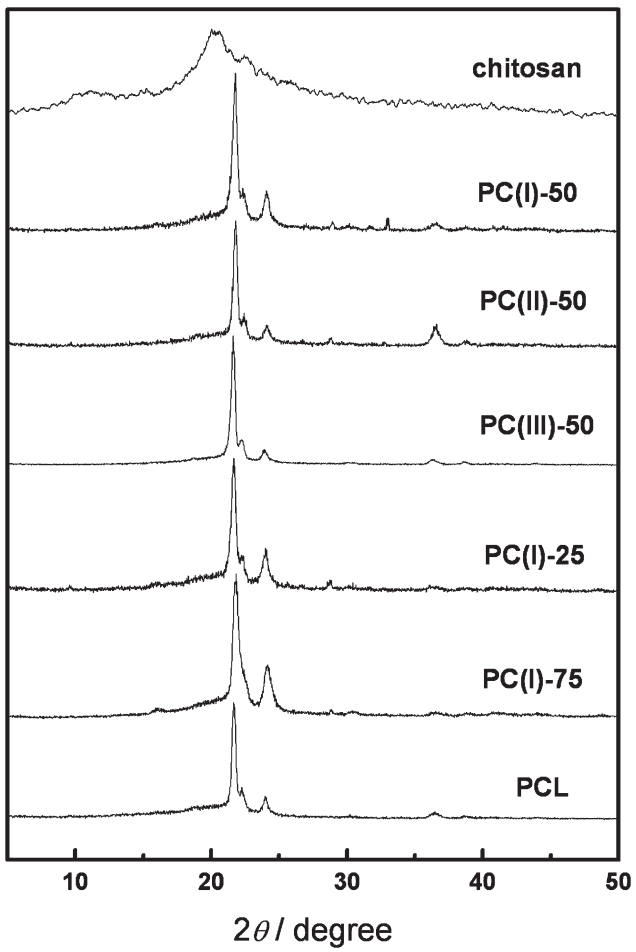

Figure 4 XRD patterns of the PC blend films, neat PCL film, and CS powder.

fraction and amorphous fraction were calculated by the division of the area of the crystalline peak or amorphous peak into the total area, which included the crystalline and amorphous peaks. Obviously, the addition of CS-*g*-PCL increased the fraction of crystalline peaks. This might be attributed to the role of CS-*g*-PCL in inducing nucleation. With an increase in the CS content in CS-*g*-PCL, the nucleation role

TABLE I
Fraction of the Carbonyl Stretching Vibration in Crystalline and Amorphous Peaks Assigned to the PCL Component Determined from the Curve-Fitting FTIR Spectra of (Figure 5) the PC Blend Films and Neat PCL Film

	Fraction of the carbonyl stretching vibration from FTIR data			
Sample	Crystalline fraction (%)	Location (cm^{-1})	Amorphous fraction (%)	Location (cm^{-1})
PCL	56.8	1722.6	43.2	1733.3
PC(I)-50	61.6	1724.6	38.4	1733.5
PC(II)-50	69.1	1724.6	30.9	1734.9
PC(III)-50	68.8	1723.5	31.2	1734.4
PC(I)-25	59.6	1723.5	40.4	1731.5
PC(I)-75	72.6	1725.0	27.4	1736.7

TABLE II
$T_{g,mid}$, ΔC_p, T_m, and ΔH_m Values from DSC Thermograms and $T_{\alpha,max}$ and $H_{loss\text{-}peak}$ Values from tan δ–Temperature Curves Assigned to the PCL Component in the PC Blends

	DSC data				DMA data	
Sample	$T_{g,mid}$ (°C)	ΔC_p (J/g K)	T_m (°C)	ΔH_m (J/g)	$T_{\alpha,max}$ (°C)	$H_{loss\text{-}peak}$
PCL	−65.0	0.167	56.8	62.24	−47.5	0.083
PC(I)-50	−65.3	0.163	57.6	70.27	−43.4	0.110
PC(II)-50	−64.7	0.136	57.6	70.41	−41.5	0.085
PC(III)-50	−66.6	0.142	57.6	74.47	−40.9	0.077
PC(I)-25	−65.0	0.156	57.8	66.74	−44.4	0.095
PC(I)-75	−65.4	0.162	57.6	69.38	−41.3	0.089

gradually became prominent and was shown as an increase in the crystalline fraction. At the same time, with an increase in the CS-*g*-PCL content in the blends, the crystalline fraction increased as well.

Thermal analysis of the PCL/CS-*g*-PCL blends

DSC and DMA were used to further understand the interaction and structure of the PCL/CS-*g*-PCL blends through the observation of the variance of domain-scale glass transitions and molecular-level α relaxations assigned to the PCL segments, respectively. Table II summarizes the glass-transition temperature at the midpoint ($T_{g,mid}$) and heat-capacity increment (ΔC_p) as well as the melting temperature (T_m) and heat enthalpy (ΔH_m) assigned to the PCL component from DSC thermograms. Meanwhile, the DSC thermograms of the PC blends and neat PCL are depicted in Figure 6. All the blends showed $T_{g,mid}$ values similar to that of the neat PCL film, and this suggested that the PCL segments in the blends and neat PCL had analogous freedom of

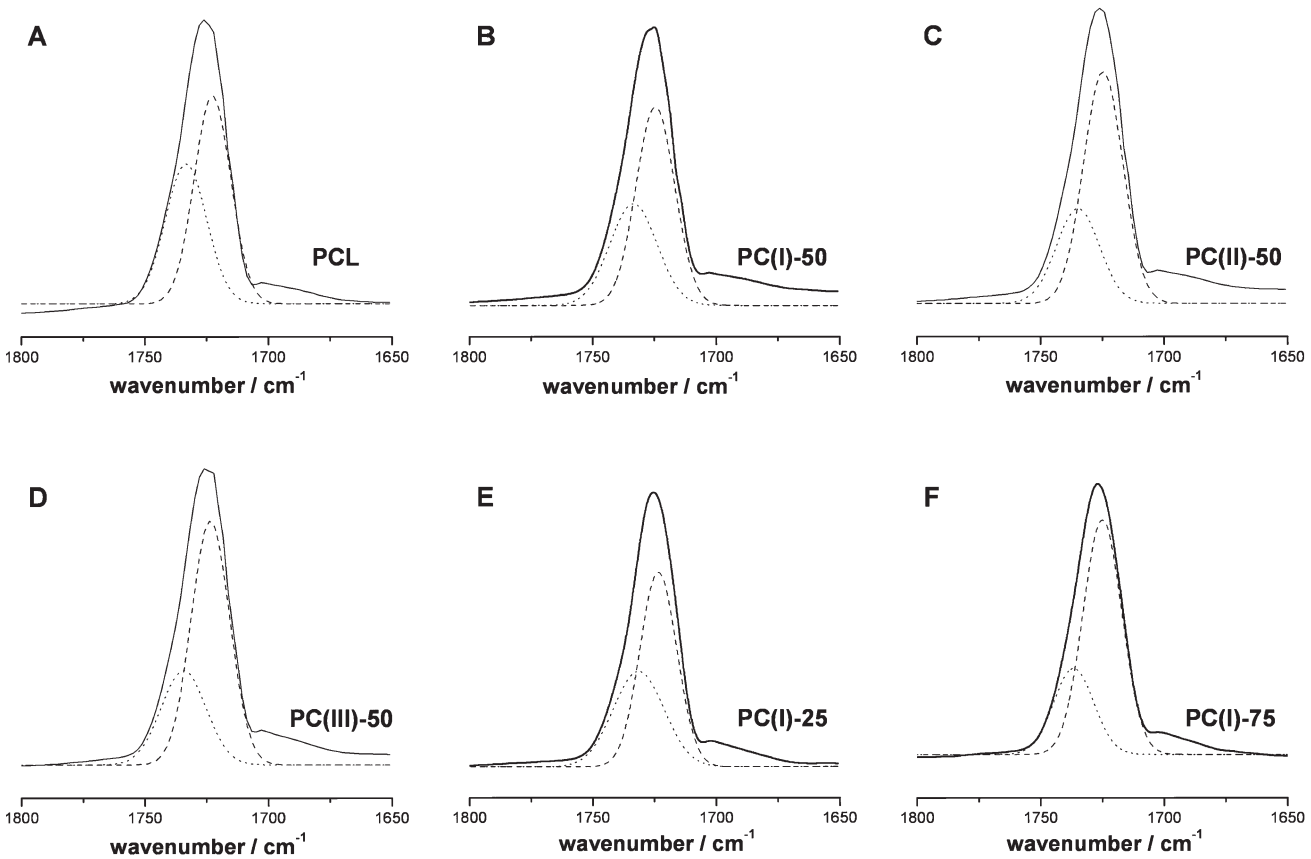

Figure 5 Experimental and curve-fitting FTIR spectra of the carbonyl stretching region assigned to the PCL component in the PC blend films and neat PCL film: (—) experimental spectrum, (- - -) crystalline part, and (· · ·) amorphous part.

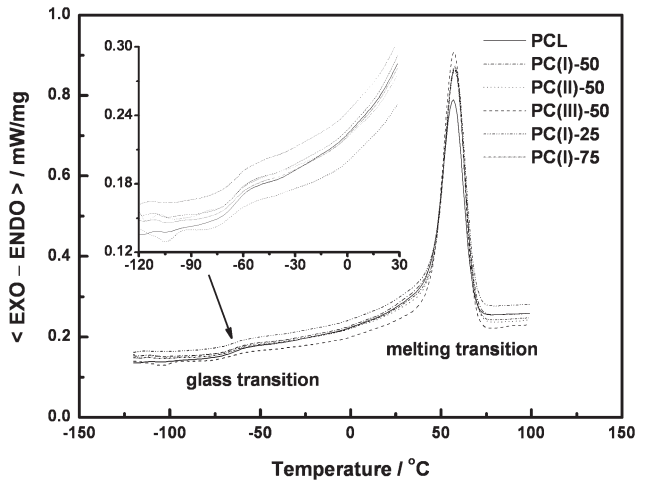

Figure 6 DSC thermograms of the PC blend films and neat PCL film.

motion on the domain scale. This was attributed to the homogeneous dissolution and improved miscibility of CS-*g*-PCL in the PCL matrix and the same origin for the grafted PCL chains and PCL matrix. In addition, the CS content was too low to show the inhibition of PCL motion on the domain scale. At the same time, higher T_m and ΔH_m values of the blends, in contrast with those of neat PCL, indicated that the crystallinity of the PCL component was improved by the nucleation role of CS-*g*-PCL. This is quite consistent with the FTIR results. Meanwhile, the higher CS content in CS-*g*-PCL and higher CS-*g*-PCL content in the blends might have facilitated the crystallinity of the PCL component in the blends; this was shown as higher ΔH_m values.

DMA is a powerful technique for reflecting the mobility of a segment through the α relaxation at the molecular level, for which the specific heat increment of the glass transition at the domain scale measured by DSC is generally ill defined. Table II summarizes the α-relaxation temperature ($T_{\alpha,\max}$) and height of the loss peak ($H_{\text{loss-peak}}$) of all the blend films and neat PCL film from the tan δ–temperature curves (Fig. 7). In contrast to no changes in the $T_{g,\text{mid}}$ values observed by DSC, the $T_{\alpha,\max}$ values of the blends were obviously higher than that of neat PCL. This suggested that the motion of the PCL segments in the blends was inhibited at the molecular level. This was attributed to covalent linkage and steric hindrance between rigid CS chains and PCL segments. Such inhibition of the PCL motion increased with an increase in the CS content in the blends; this was shown as a shift of $T_{\alpha,\max}$ values up to a high temperature for the blends containing CS-*g*-PCL with higher CS contents or containing more CS-*g*-PCL.

Fractured morphology of the PCL/CS-*g*-PCL blends

Figure 8 shows SEM images of fractured surfaces of the PC blends and neat PCL. The neat PCL had a fractured morphology with a fluctuant stripe [Fig. 8(A)] that was distinctly different from the morphology of all the blends containing CS-*g*-PCL. In contrast to neat PCL, the PC(I)-50 blends showed a porous fractured surface [Fig. 8(B)]. However, with an increase in the CS content in CS-*g*-PCL, the holes of the fractured surfaces became larger for the PC(II)-50 blends [Fig. 8(C)], and even PC(III)-50 showed a relatively smooth fractured surface [Fig. 8(D)]. This suggested that higher PCL contents in CS-*g*-PCL facilitated the uniform dispersion of CS-*g*-PCL and led to higher miscibility between CS-*g*-PCL and PCL. At this time, the most entanglement between the CS-*g*-PCL and PCL matrix existed. As a result, PC(I)-50 had the best mechanical properties. For the blends containing the same CS-*g*-PCL(I), the fractured surfaces of PC(I)-25 and PC(I)-75 [Fig. 8(E,F)] also showed a relatively smooth fractured surface similar to that of PC(III)-50 whether the CS-*g*-PCL content increased or decreased. As a result, PC(I)-50 with a moderate CS-*g*-PCL(I) content might have had the optimal miscibility between CS-*g*-PCL and PCL. However, excess CS-*g*-PCL(I), that is, 75 wt % CS-*g*-PCL(I) in the blend, resulted in a relatively brittle fractured surface, and this was shown as decreased mechanical properties and especially as the lowest elongation.

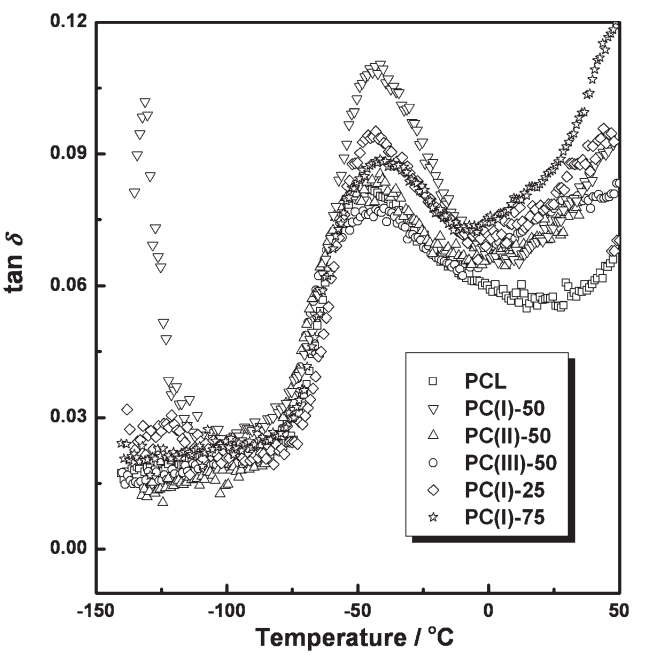

Figure 7 tan δ–temperature curves of the PC blend films and neat PCL film.

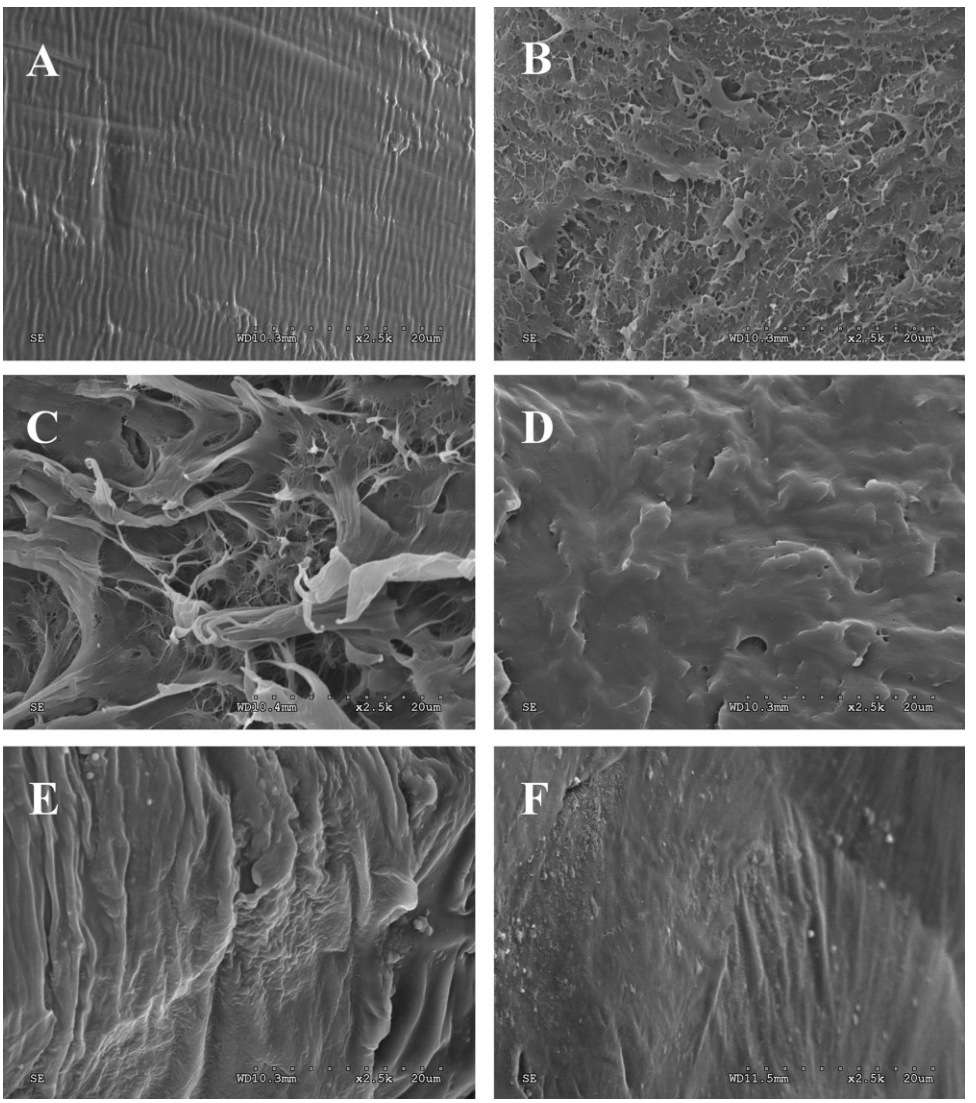

Figure 8 SEM images of fractured surfaces of the PC blend films and neat PCL film: (A) PCL, (B) PC(I)-50, (C) PC(II)-50, (D) PC(III)-50, (E) PC(I)-25, and (F) PC(I)-75.

CONCLUSIONS

As expected, CS-*g*-PCL copolymers, compounded into a PCL matrix, produced a series of composites with enhanced mechanical performance. The results showed that the strength, elongation, and Young's modulus of the resulting composites were simultaneously enhanced in contrast with those of neat PCL. Lower CS contents in CS-*g*-PCL and moderate CS-*g*-PCL contents in the blends produced the highest strength and elongation, which were about 2-fold and 3-fold greater than those of neat PCL. The addition of CS-*g*-PCL induced the nucleation of the PCL component. In combination with the rigidity of the CS chains, the strength was consequently enhanced. At the same time, the grafted PCL chains had the same origin as the PCL matrix. This improved the miscibility between the CS and PCL matrix and formed a cocontinuous interface by entanglements between the grafted PCL chains and PCL segments used as the matrix. As a result, the elongation of the composite materials was also enhanced. This work not only describes a potential type of PCL-based biomaterial with high mechanical performance and the function of CS, but also reports a strategy for enhancing the mechanical performance of composite materials.

References

1. Rinaudo, M. Prog Polym Sci 2006, 31, 603.
2. Muzzarelli, R. A. A.; Muzzarelli, C. Adv Polym Sci 2005, 186, 151.
3. Martina, A. D.; Sittinger, M.; Risbud, M. V. Biomaterials 2005, 26, 5983.
4. Kumar, M. N. V. R.; Muzzarelli, R. A. A.; Muzzarelli, C.; Sashiwa, H.; Domb, A. J. Chem Rev 2004, 104, 6017.
5. Sashiwa, H.; Aiba, S. Prog Polym Sci 2004, 29, 887.

6. Ng, K. W.; Khor, H. L.; Hutmacher, D. W. Biomaterials 2004, 25, 2807.
7. Coombes, A. G.; Rizzi, S. C.; Williamson, M.; Barralet, J. E.; Downes, S.; Wallace, W. A. Biomaterials 2004, 25, 315.
8. Amass, W. A. A.; Tighe, B. Polym Int 1998, 47, 89.
9. Tan, P. S.; Teoh, S. H. Mater Sci Eng C 2007, 27, 304.
10. Allen, C.; Han, J. N.; Yu, Y. S.; Maysinger, D.; Eisenberg, A. J Controlled Release 2000, 63, 275.
11. Woei, K.; Hutmacher, D. W.; Schantz, J. T.; Seng, C.; Too, H. P.; Chye, T.; Phan, T. T.; Teoh, S. H. Tissue Eng 2001, 7, 441.
12. Hutmacher, D. W.; Schantz, T.; Zein, I.; Ng, K. W.; Teoh, S. H.; Tan, K. C. J Biomed Mater Res 2001, 55, 203.
13. Madihally, S. V.; Matthew, H. W. Biomaterials 1999, 20, 1133.
14. Sarasam, A.; Madihally, S. V. Biomaterials 2005, 26, 5500.
15. Averous, L.; Moro, L.; Dole, P.; Fringant, C. Polymer 2000, 41, 4157.
16. Bastioli, C.; Cerutti, A.; Guanella, I.; Romano, G. C.; Tosin, M. J Environ Polym Degrad 1995, 3, 81.
17. Zhu, Y.; Gao, C.; Liu, X.; Shen, J. Biomacromolecules 2002, 3, 1312.
18. Cascone, M. G.; Barbani, N.; Cristallini, C.; Giusti, P.; Ciardelli, G.; Lazzeri, L. J Biomater Sci Polym Ed 2001, 12, 267.
19. Garcia Cruz, D. M.; Gomez Ribelles, J. L.; Salmeron Sanchez, M. J Biomed Mater Res B 2008, 85, 303.
20. Sarasam, A. R.; Krishnaswamy, R. K.; Madihally, S. V. Biomacromolecules 2006, 7, 1131.
21. Wu, C.-S. Polymer 2005, 46, 1147.
22. Sarasam, A. R.; Samli, A. I.; Hess, L.; Ihnat, M. A.; Madihally, S. V. Macromol Biosci 2007, 7, 1160.
23. She, H. D.; Xiao, X. F.; Liu, R. F. J Mater Sci 2007, 42, 8113.
24. Sarasam, A.; Madihally, S. V. Biomaterials 2005, 26, 5500.
25. Guan, X. P.; Quan, D. P.; Shuai, X. T.; Liao, K. R.; Mai, K. C. J Polym Sci Part A: Polym Chem 2007, 45, 2556.
26. Feng, H.; Dong, C. M. J Polym Sci Part A: Polym Chem 2006, 44, 5353.
27. Yu, H. J.; Wang, W. S.; Chen, X. S.; Deng, C.; Jing, X. B. Biopolymers 2006, 83, 233.
28. Liu, L.; Chen, L. X.; Fang, Y. E. Macromol Rapid Commun 2006, 27, 1988.
29. Liu, L.; Wang, Y. S.; Shen, X. F.; Fang, Y. Biopolymers 2005, 78, 163.
30. Liu, L.; Li, Y. E.; Fang, Y.; Chen, L. X. Carbohydr Polym 2005, 60, 351.
31. Liu, L.; Li, Y.; Liu, H.; Fang, Y. Eur Polym J 2004, 40, 2739.